RSC Advances

PAPER

View Article Online
View Journal | View Issue

Cite this: *RSC Adv.*, 2024, **14**, 9668

Theoretical study on the role of magnesium chloride complexes induced by different magnesium-to-chlorine ratios in magnesium–sulfur batteries

Xiaoli Jiang, Panyu Zhang, liyuan Jiang, Xinxin Zhao and Jianbao Wu *

In magnesium–sulfur batteries, electrolyte exploration is vital for developing high-energy-density, safe, and reliable batteries. This study focused on cyclic THF and chain DME, representative solvents in ether electrolytes. $MgCl_2$, an ideal anionic salt, forms mono-nuclear ($MgCl_2(DME)_2$), bi-nuclear ($[Mg_2(\mu\text{-}Cl)_2(DME)_4]^{2+}$), and tri-nuclear ($[Mg_3(\mu\text{-}Cl)_4(DME)_5]^{2+}$) complexes in DME. With increasing salt concentration, these complexes sequentially form. Under lower salt concentrations, THF and $MgCl_2$ form mono-nuclear complexes ($[MgCl_2(THF)_4]$) and continue to form bi-nuclear complexes ($[Mg_2(\mu\text{-}Cl)_3(THF)_6]^+$). However, at higher salt concentrations, bi-nuclear complexes ($[Mg_2(\mu\text{-}Cl)_3(THF)_6]^+$) directly form in THF. Comparing HOMO–LUMO values, $[Mg(DME)_3]^{2+}$ is easily oxidized. Energy gaps decrease with Cl^- ion addition, enhancing solution conductivity. Ratios of Mg^{2+} and Cl^- in S-reduction complexes differ, suggesting DME is better at a low Mg/Cl ratio, and THF at a high Mg/Cl ratio. This study contributes to understanding complexes and enhancing Mg–S battery performance.

Received 6th February 2024
Accepted 11th March 2024

DOI: 10.1039/d4ra00950a

rsc.li/rsc-advances

1. Introduction

There is an urgent need for economical, high energy density, and safe rechargeable batteries for applications in portable electronics, electric vehicles, and grid energy storage. Among potential candidates, magnesium–sulfur (Mg–S) batteries have emerged as promising contenders due to their high theoretical capacity, low cost, inherent safety, and the abundance of magnesium and sulfur in the Earth's crust. This has garnered significant research interest in recent years.[1] Mg–S batteries offer a theoretical energy density exceeding 3200 W h L^{-1}, surpassing even lithium-sulfur batteries (2800 W h L^{-1}) due to the two-electron conversion reaction $Mg^{2+} + S + 2e^- \leftrightarrow MgS$.[2–4] However, some challenges remain. Magnesium, being a highly reactive metal, presents a greater migration barrier for bivalent Mg^{2+} ions compared to traditional monovalent alkali metals. Additionally, the formation of passivation layers containing reduction products (MgO, $Mg(OH)_2$, $MgCO_3$, *etc.*) on the Mg anode hinders Mg^{2+} transfer, leading to higher impedance.[5–9] The electrolyte plays a crucial role in determining battery performance by providing the medium for ionic conduction and influencing the electrode–electrolyte interface for both cathode and anode reactions.[10] In Mg–S batteries, electrolyte additives offer a cost-effective approach to enhance performance. For instance, incorporating a small amount of I_2 facilitates Mg^{2+} transfer by forming a conductive MgI_2 layer on the Mg anode.[5] Similarly, adding $MgCl_2$ provides a readily available source of Mg ions, usually present as complexes ($MgCl^+$ or $Mg_2Cl_3^+$) in chlorine-based electrolytes. However, the dissociation of these complexes requires significant energy (around 3.0 eV).[11]

Related studies have shown that magnesium chloride complexes have excellent magnesium deposition activity and reversibility, which also helps to dissolve Mg metal passivating surface films, such as ($MgO/Mg(OH)_2$ layer.[6,10] Mg and Cl ions will form different complexes in dimethoxyethane, 2015 Cheng *et al.*[10] first proposed that the complex $[Mg_2(\mu\text{-}Cl)_2(DME)_4]^{2+}$ is formulated in dimethoxyethane (DME) through dehalodimerization of non-nucleophilic $MgCl_2$ by reacting with either Mg salts or Lewis acid salts. The results show that the complex has excellent magnesium deposition activity and reversibility. It is proved that they are feasible for practical magnesium batteries. 2017 Salama *et al.*[6] found that DME, as a ligand, can stabilize the formation of multivalent cations through intrinsically bound DME molecules, such as $[Mg_2(\mu\text{-}Cl)_2(DME)_4]^{2+}$ and $[Mg_3(\mu\text{-}Cl)_4(DME)_5]^{2+}$, which are chlorinated complexes that help to dissolve away Mg metal passivating surface films. 2017 Du *et al.*[12] identified a unique tetra-nuclear cationic complex $[Mg_4Cl_6(DME)_6]^{2+}$ for the first time and demonstrated to show high Mg plating/striping reversibility. 2019 Chaffin *et al.*[13] studied the equilibrium between *trans*-$[MgCl_2(DME)_2]$ and *cis*-$[MgCl_2(DME)_2]$ isomers using Raman and infrared spectroscopy, and indicating the presence of $[Mg_2(\mu\text{-}Cl)_2(DME)_4]^{2+}$

School of Mathematics, Physics and Statistics, Shanghai University of Engineering Science, 333 Longteng Road, Shanghai 201620, China. E-mail: wujianbao@sues.edu.cn

complex. In 2020, Huang *et al.*'s[14] study showed that the irreversible deposition of Al^{3+} leaded to an ionic configuration of magnesium trifluoromethanesulfonate based (MTB) electrolyte transformation from $[Mg_2(\mu\text{-}Cl)_2(DME)_4]^{2+}$ to $[Mg_3(\mu_3\text{-}Cl)(\mu_2\text{-}Cl)_2(DME)_7]^{3+}$ ($[Mg_2(\mu\text{-}Cl)_2(DME)_4]^{2+} + [Mg(DME)_3]^{2+} + Cl^- = [Mg_3(\mu_3\text{-}Cl)(\mu_2\text{-}Cl)_2(DME)_7]^{3+}$). 2020 Attias *et al.*[15] suggested that chlorine-containing complexes (such as $[Mg_3(\mu\text{-}Cl)_4(DME)_5]^{2+}$) adsorbed on to the Chevrel Phase (CP) surface (*e.g.*, in the 0.25 M $MgTFSI_2$ + 0.5 M $MgCl_2$/DME (ICD = Imid/Chloride/DME)) electrolyte solution) reduce the activation energy of magnesium ions in the charge transfer reaction stage across the solid/solution interface. 2021 Yang *et al.*[16] believed that the high ionic conductivity and unique solvation structure of $[Mg_2(\mu\text{-}Cl)_2(DME)_4]^{2+}$ accelerated the charge transfer process of Mg ions. 2022 Eilmes *et al.*[17] observed that besides Raman bands at 213 and 221 cm^{-1} of the respective $MgCl_2(DME)_2$ and $[Mg_2(\mu\text{-}Cl)_2(DME)_4]^{2+}$ complexes, a new band at 236 cm^{-1}, which was belonging to the $[Mg_3(\mu\text{-}Cl)_4(DME)_5]^{2+}$ species for the first time. It is suggested that the presence of both dimer and trimer could be the reason for the unprecedented electrochemical performance of the MMAC (Mg powder, $MgCl_2$ and $AlCl_3$)–DME system.

Tetrahydrofuran (THF), as a cyclic ether compound, has been widely used for its advantages of low boiling point, good fluidity, and strong solubility to many chemical substances. Studies on magnesium chloride cationic complexes have been conducted earlier. 2011 Kim *et al.*[18] studied the electrochemically active substance $[Mg_2(\mu\text{-}Cl)_3(THF)_6]^+$ formed from the reaction of an Hauser base compound HMDSMgCl and a Lewis acid $AlCl_3$. This crystallization resulted in a dramatic improvement in the potential stability and coulombic efficiency. 2014, Liu *et al.*[19] also reacted to produce $[Mg_2(\mu\text{-}Cl)_3(THF)_6]^+$ cations with electrochemical activity using the method of mono-Cl^- abstraction. This dimer has exceptional oxidation stability, improved electrophilic susceptibility, high current density and reversible Mg plating and stripping. 2015, Liu *et al.*[20] believed that $[Mg_2(\mu\text{-}Cl)_3(THF)_6]^+$ and $[MgCl(THF)_3]^+$ could both be used as active substances for Mg deposition. 2015 See *et al.*[21] suggested that the active Mg complex in conditioned magnesium aluminum chloride complex (MACC) is very likely the $[Mg_2(\mu\text{-}Cl)_3(THF)_6]^+$ complex that is observed in the solid state structure. Later See *et al.* confirmed in 2017[22] that $[Mg_2(\mu\text{-}Cl)_3(THF)_6]^+$ is the main active complex for Mg electrodeposition, and the higher the concentrations, the higher the deposition currents. 2019, B. Moss *et al.*'s,[23] calculation results showed that $MgCl_2(THF)_3$ dichloride species and $[MgCl(THF)_5]^+$ monochloride species are the dominant mononuclear species in solution, and they combine to form a binuclear species $[Mg_2(\mu\text{-}Cl)_3(THF)_6]^+$. Both mono-cation species can act as active species for Mg deposition, but the dinuclear species in the electrolyte have significant dominance and it is the primary species involved in reversible Mg deposition. 2020, Chaffin *et al.*'s,[24] spectral results showed that $[Mg(THF)_6]^{2+}$ is the major species and responsible for the lower electrochemical performance of the 1 : 1 MACC-THF electrolyte, whereas $[MgCl_2(THF)_4]$ and $[Mg_2(\mu\text{-}Cl)_3(THF)_6]^+$ are the complexes related with the higher electrochemical activity of the 2 : 1 MACC-THF electrolyte. 2021 Eilmes *et al.*[25] also proved the research results of Chaffin, and also proposed the existence of $[MgCl(THF)_5]^+$ complex in the electrolyte solvent of 1 : 1 MACC-THF. By calculating the infrared spectrum, it is also shown that $[MgCl(THF)_5]^+$ and $[Mg_2(\mu\text{-}Cl)_3(THF)_6]^+$ preferentially formed at in 1 : 1 and 2 : 1 electrolyte solutions, respectively. 2022 Xiao *et al.*[26] formed an all-magnesium salt electrolyte by co-dissolving $Mg(pftb)_2$ and $MgCl_2$ in THF. Complex $[Mg_2(\mu\text{-}Cl)_3(THF)_6]^+$ is the main electrochemically active species of the electrolyte. The higher $MgCl_2$ concentration, corresponding to more active ions $[Mg_2(\mu\text{-}Cl)_3(THF)_6]^+$, gives higher redox reaction current density. 2022 Cheng *et al.*[27] found that the chlorine-containing cation in the novel $MgCl_2$–$B(Otfe)_3$ (MCBB) electrolyte is $[Mg_2(\mu\text{-}Cl)_2(THF)_6]^{2+}$, which has a lower de-solvation energy barrier in terms of Mg plating.

The above studies show that different proportions and concentrations of Mg^{2+} and Cl^- in solution will produce different types of cations, which will have different effects on deposition overpotential, current density and regulation process. The related literature show that, Mg/Cl = 1 : 1 corresponds to $MgCl^+$,[20,23,25] $Mg_2Cl_2^{2+}$,[6,10,13,14,16,17,27] $Mg_3Cl_3^{3+}$ (ref. 14) cations, Mg/Cl = 1 : 2 corresponds to $MgCl_2$,[13,17,23,24] Mg/Cl = 2 : 3 corresponds to $Mg_2Cl_3^+$,[18–26] $Mg_4Cl_6^{2+}$ (ref. 12) cations, and Mg/Cl = 3 : 4 corresponds to $Mg_3Cl_4^{2+}$ (ref. 6, 15 and 17) cations. These cations combine with different solvent molecules (such as DME or THF) to form different complexes, which have the effect of improving the battery interface and improving the battery performance. The degree of de-solvation of Mg ions from the electrolyte is an important factor affecting the performance of Mg–S batteries, but the mechanism of the interaction between the magnesium anode and the electrolyte interface is still unclear. The generation process of these magnesium chloride complexes and the thermodynamic behavior in the discharge process have not been studied systematically.

In this paper, we first determined the stable complex structures of different anions and Mg^{2+} in DME solution by calculation. It was observed that Cl^- had a better de-solvation effect on Mg^{2+} in solvent. Then, the structure and properties of magnesium chloride complexes formed in DME and THF electrolytes were investigated in detail according to the different proportion of Mg/Cl. According to the concentration of Mg/Cl in different proportions, we determined the magnesium chloride cationic complexes in different solvents. The DME molecule has a di-oxygen chain structure, forming the $[Mg_2(\mu\text{-}Cl)_2(DME)_4]^{2+}$ complex at Mg/Cl = 1 : 1, the $[Mg_3(\mu\text{-}Cl)_4(DME)_5]^{2+}$ complex at Mg/Cl = 3 : 4. THF has a mono-oxygen ring structure, forming the $[MgCl_2(THF)_4]$ complex at Mg/Cl = 1 : 2, the $[Mg_2(\mu\text{-}Cl)_3(THF)_6]^+$ complex at Mg/Cl = 2 : 3. According to the free energy calculation results, we analyzed the formation process of magnesium chloride complexes. With the increase of $MgCl_2$ salt concentration, the proportion of Mg/Cl also increased, and $MgCl_2(DME)_2$ was first formed in DME solution. With the increase of $MgCl_2$ salt concentration, the main complex in the solution was $[Mg_2(\mu\text{-}Cl)_2(DME)_4]^{2+}$, and as $MgCl_2$ continues to increase, the reaction mainly produces $[Mg_3(\mu\text{-}Cl)_4(DME)_5]^{2+}$ complex. Similarly, the $[MgCl_2(THF)_4]$ complex was first formed in THF solution, and with the increase of salt, the main complex

becomes $[Mg_2(\mu\text{-}Cl)_3(THF)_6]^+$. In addition, we drew a flow chart of the action of magnesium chloride complexes in the process of S-reduction under different solvation conditions. In contrast, the Mg/Cl ratio in DME is lower, while the Mg/Cl ratio in THF is higher. If the two solvents are mixed, then the Mg/Cl ratio of the electrolyte can be kept constant.

2. Computational methods

In order to find the preferred structures of magnesium chloride complexes, we employed the swarm-intelligence based ABCluster structure prediction method,[28,29] which can efficiently search for the stable structures. Furthermore, a global search should be an effective method to avoid missing candidates of ground state structures. To improve the search efficiency, point group symmetry and the bond characterization matrix technique were included to eliminate similar structures.

The underlying local structure optimization and electronic property calculations were performed at the density functional theory (DFT) level using the B3LYP[30] hybrid functional as implemented in the Gaussian 16 package. Since there are thousands of structures generated during the structure search, an economic basis set, *i.e.* 3-21G for Mg and S, was chosen to optimize these structures. These settings are enough for evaluating the relative energies of the generated structures. After the structure search, the accurate basis set of 3-21+G(d) was used for the refined structure optimization and vibrational frequency calculation for the isomers with low-lying energies. The absence of an imaginary frequency confirms that the predicted structures are stability.

First, we calculated the reaction voltage per solvent molecule, the formation energies were defined as

$$\Delta G_b^{solven} = G^{solven}_{[Mg_xCl_y(DME/THF)_n]^{(2x-y)+}} - G^{solven}_{MgCl_2} - G^{solven}_{DME/THF} - G^{solven}_{Mg^{2+}} \quad (1)$$

where $G_{[Mg_xCl_y(DME/THF)_n]^{(2x-y)+}}$ is the lowest energy of structure $Mg_xCl_y(DME/THF)_n$, E_{MgCl_2} and $G_{DME/THF}$ are the energy of $MgCl_2$ and DME/THF molecule respectively. And $G_{Mg}{}^{2+}$ is the energy of magnesium ion. All the energies involved in the calculation in eqn (1) are based on the solvent environment of 1,2-dimethoxy-ethane (DME) and 1,4-epoxybutane (THF). In addition, the implicit solvent method is used ($\varepsilon = 7.2$ (DME) and $\varepsilon = 7.6$ (THF)).

The Gibbs reaction free energy is defined as

$$\Delta G = E_{resultant} - E_{reactant} \quad (2)$$

where $E_{resultant}$ is the energy of the resultant, $E_{reactant}$ is the energy of the reactants.

The change in the driving force of the Gibbs reaction is defined as

$$\Delta^2 G = \Delta G_{Rx} - \Delta G_{Ry} \quad (3)$$

where ΔG_{Rx} and ΔG_{Ry} are the Gibbs free energies of the corresponding equation.[31]

HOMO–LUMO energy gap (E_g) was calculated as follows

$$E_g = E_{LUMO} - E_{HOMO} \quad (4)$$

Among them, E_{LUMO} and E_{HOMO} are the energy levels of LUMO and HOMO, respectively.

3. Results and discussion

3.1 Effect of different anions within DME solvent on the desolvation of Mg^{2+}

Magnesium sulfur battery electrolyte solute anions are numerous, corresponding to the formation of different complexes, before the study of the exact complex mechanism need to determine the appropriate anion, which has practical

Table 1 The different anions in DME solvent form stable structures with Mg^{2+}, and the stable structure of Mg–Cl complexes in DME and THF solvents

No. 1	No. 2	No. 3	No. 4
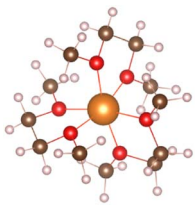	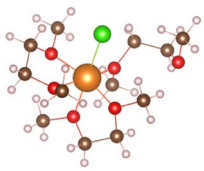	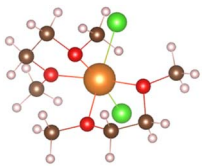	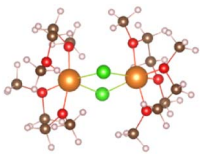
$[Mg(DME)_3]^{2+}$	$[MgCl(DME)_3]^+$	$MgCl_2(DME)_2$	$[Mg_2(\mu\text{-}Cl)_2(DME)_4]^{2+}$
No. 5	No. 6	No. 7	No. 8
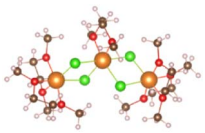	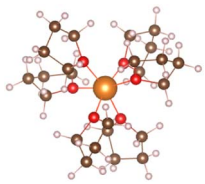	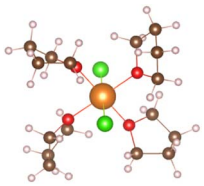	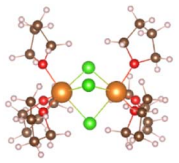
$[Mg_3(\mu\text{-}Cl)_4(DME)_5]^{2+}$	$[Mg(THF)_6]^{2+}$	$MgCl_2(THF)_4$	$[Mg_2(\mu\text{-}Cl_3)(THF)_6]^+$

significance to put into production in later stage, we have done research on several suitable anions, by adding anions in the solvent stable structures as shown in the Table below.

From the stable structure of $[Mg(DME)_3]^{2+}$ without anion added in Table 1, it can be seen that the oxygen atom coordination number around Mg ion is 6. Table 1 shows the stable structures of adding one Cl^- ion (No. 2) and two Cl^- ions (No. 3). It can be seen that Cl atoms replace the position of oxygen atoms and form Mg–Cl bond, indicating that Cl^- can have a better de-solvation effect on Mg^{2+} at DME solvent, help to increase the solubility of Mg^{2+} and improve the performance of Mg–S battery. In the following, we will focus on the structures and formation process of Mg–Cl complexes of $MgCl_2$ salt solute in different electrolytes (DME, THF) according to Mg/Cl ratio.

3.2 Structures and formation process of $MgCl_2$ solute within DME solvent

The structure of different Mg–Cl complexes in DME solvent are shown in the Table 1. We first found the lowest energy stable complex structures through calculation, and the results are shown in the Table 1.

According to the Mg/Cl = 1 : 1, Mg/Cl = 1 : 1.3 and Mg/Cl = 1 : 2, the three structures can be obtained in Table 1. From the structures in Table 1, it seen that the mono-nuclear complex (No. 3) of Mg atom is composed of four Mg–O bonds and two Mg–Cl bonds, with a total coordination number of 6. It can be seen from the structures of bi-nuclear (No. 4) and tri-nuclear complex (No. 5) that two chlorine atoms are shared between the two magnesium atoms, and the remaining coordination are complemented by the oxygen atoms in the DME. The stable structures we found based on the DFT calculation are consistent with the structures in the previous literature.[6]

3.2.1 Formation path of Mg–Cl complexes within DME solution. In the above, we have obtained the lowest energy structure of mono-nuclear, bi-nuclear and tri-nuclear complexes, but the formation process and reaction mechanism of each complex are still not well understood. Therefore, we predict the reaction generation paths of several complexes, as shown in Table 2 below.

We studied the reaction mechanism of Mg–Cl cationic ligands to form complexes in DME. The results of the free energy are calculated with the eqn (1), and the simulation show that the possible reactions between $MgCl_2$ and four DME molecules and the corresponding reaction free energy are shown in Fig. 1. One reaction pathway is that with the addition of $MgCl_2$, $MgCl_2(DME)_2$, $[Mg_2(\mu\text{-}Cl)_2(DME)_4]^{2+}$ and $[Mg_3(\mu\text{-}Cl)_4(DME)_5]^{2+}$ complexes gradually appear in the solution. The other is to form $MgCl_2(DME)_2$ complex in solution first, then react with Mg ion in solution to form $[Mg_2(\mu\text{-}Cl)_2(DME)_4]^{2+}$, and then continue to react with $MgCl_2$ salt to form $[Mg_3(\mu\text{-}Cl)_4(DME)_5]^{2+}$. As shown in step R_1, the reaction between $MgCl_2$ and DME produces the intermediate $MgCl_2(DME)_2$, where calculated free energy (ΔG) is −4.31 eV, and then $MgCl_2$ increases to produce $[Mg_2(\mu\text{-}Cl)_2(DME)_4]^{2+}$ complex, as shown in step R_4. The free energy of the process is −1.17 eV. $MgCl_2$ salt continues to increase the reaction to form the $[Mg_3(\mu\text{-}Cl)_4(DME)_5]^{2+}$ complex, which ΔG is −0.84 eV, as shown in step R_5. Others reaction method, such as R_2 and R_3, ΔG are all over 0 for $[Mg_2(\mu\text{-}Cl)_2(DME)_4]^{2+}$ and $[Mg_3(\mu\text{-}Cl)_4(DME)_5]^{2+}$, indicating that the reaction is difficult to occur. The reaction shown in R_1, R_4, and R_5 is more favorable. And mono-nuclear, bi-nuclear, and tri-nuclear complexes are formed directly in the electrolyte solution with the increase of $MgCl_2$ salt.

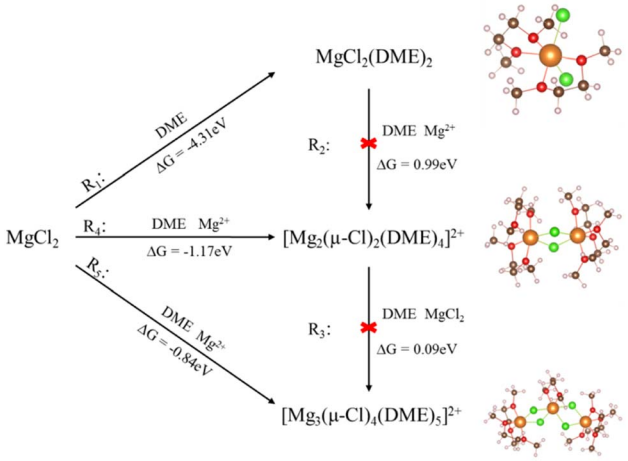

Fig. 1 Reaction pathways of Mg–Cl complexes in DME solvent.

3.2.2 The Mg–Cl complexes within DME solution in the process of discharge reaction. The positive electrode is a very important part of the Mg–S battery system, so we studied the reaction of the positive electrode of sulfur, according to the change of the valence of sulfur, we listed the following reaction equation, and calculated the corresponding reaction free energy ΔG.

All the calculation results in Table 3 are obtained under the conditions of DME solvation. As can be seen from Table 3, the magnesium polysulfide involved in the calculation are the structures energy optimized in the previous work,[32] the ΔG of R_{13} is under 0, which can be occurred spontaneously, while the free energy of the rest R_6–R_{12} are over 0, As mentioned above,

Table 2 Reaction steps to form mono-nuclear, bi-nuclear, and tri-nuclear complexes in DME solutions

No.	Equation	ΔG (eV)	$\Delta G_{per\ DME}$
R_1	$MgCl_2 + 2DME = MgCl_2(DME)_2$	−8.62	−4.31
R_2	$Mg^{2+} + MgCl_2(DME)_2 + 2DME = [Mg_2(\mu\text{-}Cl)_2(DME)_4]^{2+}$	3.95	0.99
R_3	$MgCl_2 + [Mg_2(\mu\text{-}Cl)_2(DME)_4]^{2+} + DME = [Mg_3(\mu\text{-}Cl)_4(DME)_5]^{2+}$	0.46	0.09
R_4	$Mg^{2+} + MgCl_2 + 4DME = [Mg_2(\mu\text{-}Cl)_2(DME)_4]^{2+}$	−4.67	−1.17
R_5	$Mg^{2+} + 2MgCl_2 + 5DME = [Mg_3(\mu\text{-}Cl)_4(DME)_5]^{2+}$	−4.21	−0.84

Table 3 Reaction equation for the formation of magnesium polysulfides and tri-nuclear complex within DME solution by bi-nuclear complex and sulfur anion

No.	Equation	ΔG (eV)	$\Delta G_{\text{per S}}$
R_6	$S_8^{2-} + 2[Mg_2(\mu\text{-}Cl)_2(DME)_4]^{2+} = MgS_8 + [Mg_3(\mu\text{-}Cl)_4(DME)_5]^{2+} + 3DME$	1.86	0.23
R_7	$S_7^{2-} + 2[Mg_2(\mu\text{-}Cl)_2(DME)_4]^{2+} = MgS_7 + [Mg_3(\mu\text{-}Cl)_4(DME)_5]^{2+} + 3DME$	1.82	0.26
R_8	$S_6^{2-} + 2[Mg_2(\mu\text{-}Cl)_2(DME)_4]^{2+} = MgS_6 + [Mg_3(\mu\text{-}Cl)_4(DME)_5]^{2+} + 3DME$	1.67	0.28
R_9	$S_5^{2-} + 2[Mg_2(\mu\text{-}Cl)_2(DME)_4]^{2+} = MgS_5 + [Mg_3(\mu\text{-}Cl)_4(DME)_5]^{2+} + 3DME$	1.55	0.31
R_{10}	$S_4^{2-} + 2[Mg_2(\mu\text{-}Cl)_2(DME)_4]^{2+} = MgS_4 + [Mg_3(\mu\text{-}Cl)_4(DME)_5]^{2+} + 3DME$	1.29	0.32
R_{11}	$S_3^{2-} + 2[Mg_2(\mu\text{-}Cl)_2(DME)_4]^{2+} = MgS_3 + [Mg_3(\mu\text{-}Cl)_4(DME)_5]^{2+} + 3DME$	0.80	0.27
R_{12}	$S_2^{2-} + 2[Mg_2(\mu\text{-}Cl)_2(DME)_4]^{2+} = MgS_2 + [Mg_3(\mu\text{-}Cl)_4(DME)_5]^{2+} + 3DME$	0.11	0.05
R_{13}	$S^{2-} + 2[Mg_2(\mu\text{-}Cl)_2(DME)_4]^{2+} = MgS + [Mg_3(\mu\text{-}Cl)_4(DME)_5]^{2+} + 3DME$	−1.49	−1.49

MgS MgS_2 MgS_3 MgS_4 MgS_5 MgS_6 MgS_7 MgS_8

Table 4 Reaction of bi-nuclear to tri-nuclear complexes during S-reduction within DME solution

No.	Equation	ΔG (eV)	$\Delta G_{\text{per S}}$
R_{14}	$3S_8^{2-} + 2[Mg_2(\mu\text{-}Cl)_2(DME)_4]^{2+} + 2e^- = 3S_6^{2-} + [Mg_3(\mu\text{-}Cl)_4(DME)_5]^{2+} + 3DME + MgS_6$	−5.57	−0.23
R_{15}	$2S_6^{2-} + 2[Mg_2(\mu\text{-}Cl)_2(DME)_4]^{2+} + 2e^- = 2S_4^{2-} + [Mg_3(\mu\text{-}Cl)_4(DME)_5]^{2+} + 3DME + MgS_4$	−5.18	−0.43
R_{16}	$S_4^{2-} + 2[Mg_2(\mu\text{-}Cl)_2(DME)_4]^{2+} + 2e^- = S_2^{2-} + [Mg_3(\mu\text{-}Cl)_4(DME)_5]^{2+} + 3DME + MgS_2$	−4.13	−1.03
R_{17}	$S_2^{2-} + 2[Mg_2(\mu\text{-}Cl)_2(DME)_4]^{2+} + 2e^- = S^{2-} + [Mg_3(\mu\text{-}Cl)_4(DME)_5]^{2+} + 3DME + MgS$	−3.01	−1.50

both $[Mg_2(\mu\text{-}Cl)_2(DME)_4]^{2+}$ and $[Mg_3(\mu\text{-}Cl)_4(DME)_5]^{2+}$ are directly formed in solution and do not undergo spontaneous transformation. If the reaction of R_6–R_{12} are required, we assume that external forces may be needed to assist it, such as adding catalysts or additives.

3.2.3 Effect of Mg–Cl complexes on S-reduction process within DME solution. As shown in Table 4, the positive anion of sulfur initially exists in solution in the form of S_8^{2-}, and reacts with the bi-nuclear complex $[Mg_2(\mu\text{-}Cl)_2(DME)_4]^{2+}$ in the first step to form the tri-nuclear complex $[Mg_3(\mu\text{-}Cl)_4(DME)_5]^{2+}$ and S_6^{2-} anion. In the second step, the S_6^{2-} anion continues to react with the bi-nuclear complex $[Mg_2(\mu\text{-}Cl)_2(DME)_4]^{2+}$ to form the tri-nuclear complex $[Mg_3(\mu\text{-}Cl)_4(DME)_5]^{2+}$ and S_4^{2-} anion. In the third step, the S_4^{2-} anion continues to react with the bi-nuclear complex $[Mg_2(\mu\text{-}Cl)_2(DME)_4]^{2+}$ to form the tri-nuclear complex $[Mg_3(\mu\text{-}Cl)_4(DME)_5]^{2+}$ and S_2^{2-}anion. The fourth step S_2^{2-} anion continues to react with the bi-nuclear complex $[Mg_2(\mu\text{-}Cl)_2(DME)_4]^{2+}$ to form the tri-nuclear complex $[Mg_3(\mu\text{-}Cl)_4(DME)_5]^{2+}$ and S^{2-} anion. Tables 5–7 show the decomposition of complexes involved in the S-reduction reaction.

3.3 Structures and formation process of $MgCl_2$ solute within THF solvent

According to the Mg/Cl ratios of 1 : 0, 1 : 1.5 and 1 : 2, the relevant THF complex structures in Table 1 are obtained. It can be

Table 5 Reaction of bi-nuclear to mono-nuclear complexes during S-reduction within DME solution

No.	Equation	ΔG (eV)	$\Delta G_{\text{per S}}$
R_{18}	$3S_8^{2-} + [Mg_2(\mu\text{-}Cl)_2(DME)_4]^{2+} + 2e^- = 3S_6^{2-} + MgCl_2(DME)_2 + 2DME + MgS_6$	−14.64	−0.61
R_{19}	$2S_6^{2-} + [Mg_2(\mu\text{-}Cl)_2(DME)_4]^{2+} + 2e^- = 2S_4^{2-} + MgCl_2(DME)_2 + 2DME + MgS_4$	−14.26	−1.19
R_{20}	$S_4^{2-} + [Mg_2(\mu\text{-}Cl)_2(DME)_4]^{2+} + 2e^- = S_2^{2-} + MgCl_2(DME)_2 + 2DME + MgS_2$	−13.20	−3.30
R_{21}	$S_2^{2-} + [Mg_2(\mu\text{-}Cl)_2(DME)_4]^{2+} + 2e^- = S^{2-} + MgCl_2(DME)_2 + 2DME + MgS$	−12.08	−6.04

Table 6 Reaction of tri-nuclear to mono-nuclear complexes during S-reduction within DME solution

No.	Equation	ΔG (eV)	$\Delta G_{\text{per S}}$
R_{22}	$3S_8^{2-} + [Mg_3(\mu\text{-}Cl)_4(DME)_5]^{2+} + 2e^- = 3S_6^{2-} + 2MgCl_2(DME)_2 + DME + MgS_6$	−23.71	−0.99
R_{23}	$2S_6^{2-} + [Mg_3(\mu\text{-}Cl)_4(DME)_5]^{2+} + 2e^- = 2S_4^{2-} + 2MgCl_2(DME)_2 + DME + MgS_4$	−23.33	−1.94
R_{24}	$S_4^{2-} + [Mg_3(\mu\text{-}Cl)_4(DME)_5]^{2+} + 2e^- = S_2^{2-} + 2MgCl_2(DME)_2 + DME + MgS_2$	−22.27	−5.57
R_{25}	$S_2^{2-} + [Mg_3(\mu\text{-}Cl)_4(DME)_5]^{2+} + 2e^- = S^{2-} + 2MgCl_2(DME)_2 + DME + MgS$	−21.15	−10.58

Table 7 Reaction of tri-nuclear to bi-nuclear complexes during S-reduction within DME solution

No.	Equation	ΔG (eV)	$\Delta G_{per\ S}$
R_{26}	$3S_8^{2-} + Mg^{2+} + [Mg_3(\mu\text{-}Cl)_4(DME)_5]^{2+} + 3DME + 2e^- = 4S_6^{2-} + 2[Mg_2(\mu\text{-}Cl)_2(DME)_4]^{2+}$	−12.36	−0.52
R_{27}	$2S_6^{2-} + Mg^{2+} + [Mg_3(\mu\text{-}Cl)_4(DME)_5]^{2+} + 3DME + 2e^- = 3S_4^{2-} + 2[Mg_2(\mu\text{-}Cl)_2(DME)_4]^{2+}$	−11.60	−0.97
R_{28}	$S_4^{2-} + Mg^{2+} + [Mg_3(\mu\text{-}Cl)_4(DME)_5]^{2+} + 3DME + 2e^- = 2S_2^{2-} + 2[Mg_2(\mu\text{-}Cl)_2(DME)_4]^{2+}$	−9.36	−2.34
R_{29}	$S_2^{2-} + Mg^{2+} + [Mg_3(\mu\text{-}Cl)_4(DME)_5]^{2+} + 3DME + 2e^- = 2S^{2-} + 2[Mg_2(\mu\text{-}Cl)_2(DME)_4]^{2+}$	−6.64	−3.32

Table 8 Reaction steps to form mono-nuclear and bi-nuclear complexes within THF solution

No.	Equation	ΔG (eV)	$\Delta G_{per\ THF}$
R_{30}	$MgCl_2 + 4THF = MgCl_2(THF)_4$	−9.02	−2.25
R_{31}	$Mg^{2+} + 3MgCl_2(THF)_4 = 2[Mg_2(\mu\text{-}Cl)_3(THF)_6]^+$	−6.32	−0.53
R_{32}	$Mg^{2+} + 3MgCl_2 + 12THF = 2[Mg_2(\mu\text{-}Cl)_3(THF)_6]^+$	−33.37	−2.78

seen that $[Mg(THF)_6]^{2+}$ (No. 6) is composed of one Mg ion and six THF molecules. THF are symmetrically distributed around Mg ion, and the total coordination number of Mg ion is 6. In addition, the THF pairs cross vertically in space, which can helps the structure remain stable. $MgCl_2(THF)_4$ (No. 7) consists of one magnesium atom and two chlorine atoms to form a mono-nuclear complex with Mg coordination number of 6, $[Mg_2(\mu\text{-}Cl)_3(THF)_6]^+$ (No. 8) shares three chlorine atoms between two magnesium atoms, and the remaining magnesium atoms are complemented by three oxygen atoms in the THF molecules to form a bi-nuclear complex. (This structure is consistent with that reported in earlier literature[22]). The chlorine atoms replace the oxygen atoms well and significantly enhance the de-solvation of the magnesium atoms. Moreover, the three structures in Table 1 are highly symmetrical.

3.3.1 Formation path of Mg–Cl complexes within THF solution. According to the calculation results in Table 8, the bi-nuclear complex $[Mg_2(\mu\text{-}Cl)_3(THF)_6]^+$ in THF solution is directly formed under the condition of high salt concentration, as shown in R_{32}, and the reaction free energy is −2.78 eV. When the salt concentration is not that high, mono-nuclear complex $[MgCl_2(THF)_4]$ is formed at first, which ΔG is −2.25 eV, as shown in R_{30}. Then it continues to react with $MgCl_2$ to form a bi-nuclear complex $[Mg_2(\mu\text{-}Cl)_3(THF)_6]^+$, as shown in R_{31}.

3.3.2 The Mg–Cl complexes within THF solution in the process of discharge reaction. The calculated results of all the above steps are obtained under the condition of THF solvation. It can be seen from Table 9 that the free energies of R_{33}–R_{40} are all under 0, indicating that all the reactions of the above steps can be occurred spontaneously.

3.3.3 Effect of Mg–Cl complexes on S-reduction process within THF solution. It can be seen from Table 10, that the conversion of the mono-nuclear complex to the bi-nuclear complex in THF solution can occur spontaneously in the S-reduction reaction. The free energy of R_{41}–R_{44} are all under 0, $\Delta G_{per\ S}$ of R_{41} is −0.71 eV, R_{42} is −1.38 eV, R_{43} is −3.87 eV, R_{44} is

Table 9 Reaction equation for the formation of magnesium polysulfides and bi-nuclear complex within THF solution by mono-nuclear complex and sulfur anion

No.	Equation	ΔG (eV)	$\Delta G_{per\ S}$
R_{33}	$S_8^{2-} + 2Mg^{2+} + 3[MgCl_2(THF)_4] = MgS_8 + 2[Mg_2(\mu\text{-}Cl)_3(THF)_6]^+$	−9.44	−1.18
R_{34}	$S_7^{2-} + 2Mg^{2+} + 3[MgCl_2(THF)_4] = MgS_7 + 2[Mg_2(\mu\text{-}Cl)_3(THF)_6]^+$	−9.46	−1.35
R_{35}	$S_6^{2-} + 2Mg^{2+} + 3[MgCl_2(THF)_4] = MgS_6 + 2[Mg_2(\mu\text{-}Cl)_3(THF)_6]^+$	−9.61	−1.60
R_{36}	$S_5^{2-} + 2Mg^{2+} + 3[MgCl_2(THF)_4] = MgS_5 + 2[Mg_2(\mu\text{-}Cl)_3(THF)_6]^+$	−9.73	−1.95
R_{37}	$S_4^{2-} + 2Mg^{2+} + 3[MgCl_2(THF)_4] = MgS_4 + 2[Mg_2(\mu\text{-}Cl)_3(THF)_6]^+$	−10.00	−2.50
R_{38}	$S_3^{2-} + 2Mg^{2+} + 3[MgCl_2(THF)_4] = MgS_3 + 2[Mg_2(\mu\text{-}Cl)_3(THF)_6]^+$	−10.48	−3.49
R_{39}	$S_2^{2-} + 2Mg^{2+} + 3[MgCl_2(THF)_4] = MgS_2 + 2[Mg_2(\mu\text{-}Cl)_3(THF)_6]^+$	−11.17	−5.59
R_{40}	$S^{2-} + 2Mg^{2+} + 3[MgCl_2(THF)_4] = MgS + 2[Mg_2(\mu\text{-}Cl)_3(THF)_6]^+$	−12.76	−12.76

Table 10 Reaction of mono-nuclear to bi-nuclear complexes within THF solution during S-reduction

No.	Equation	ΔG (eV)	$\Delta G_{per\ S}$
R_{41}	$3S_8^{2-} + 2Mg^{2+} + 3[MgCl_2(THF)_4] + 2e^- = 3S_6^{2-} + 2[Mg_2(\mu\text{-}Cl)_3(THF)_6]^+ + MgS_6$	−16.96	−0.71
R_{42}	$2S_6^{2-} + 2Mg^{2+} + 3[MgCl_2(THF)_4] + 2e^- = 2S_4^{2-} + 2[Mg_2(\mu\text{-}Cl)_3(THF)_6]^+ + MgS_4$	−16.53	−1.38
R_{43}	$S_4^{2-} + 2Mg^{2+} + 3[MgCl_2(THF)_4] + 2e^- = S_2^{2-} + 2[Mg_2(\mu\text{-}Cl)_3(THF)_6]^+ + MgS_2$	−15.50	−3.87
R_{44}	$S_2^{2-} + 2Mg^{2+} + 3[MgCl_2(THF)_4] + 2e^- = S^{2-} + 2[Mg_2(\mu\text{-}Cl)_3(THF)_6]^+ + MgS$	−14.38	−7.19

Table 11 Reaction of bi-nuclear to mono-nuclear complexes during S-reduction within THF solution

No.	Equation	ΔG (eV)	$\Delta G_{\text{per S}}$
R_{45}	$3S_8^{2-} + 2[Mg_2(\mu\text{-}Cl)_3(THF)_6]^+ + 2e^- = 3S_6^{2-} + 3[MgCl_2(THF)_4] + MgS_6$	−4.31	−0.18
R_{46}	$2S_6^{2-} + 2[Mg_2(\mu\text{-}Cl)_3(THF)_6]^+ + 2e^- = 2S_4^{2-} + 3[MgCl_2(THF)_4] + MgS_4$	−3.88	−0.32
R_{47}	$S_4^{2-} + 2[Mg_2(\mu\text{-}Cl)_3(THF)_6]^+ + 2e^- = S_2^{2-} + 3[MgCl2(THF)4] + MgS_2$	−2.85	−0.71
R_{48}	$S_2^{2-} + 2[Mg_2(\mu\text{-}Cl)_3(THF)_6]^+ + 2e^- = S^{2-} + 3[MgCl_2(THF)_4] + MgS$	−1.73	−0.87

−7.19 eV. It indicates that R_{41}–R_{44} reaction are more and more easily to occur. Table 11 shows the decomposition of complexes involved in the S-reduction reaction.

3.4 Properties of Mg–Cl complexes within DME and THF solvents

For complexes of $[Mg(DME)_3]^{2+}$, $[MgCl(DME)_3]^+$, $MgCl_2(DME)_2$, $[Mg_2(\mu\text{-}Cl_2)(DME)_4]^{2+}$ and $[Mg_3(\mu\text{-}Cl_4)(DME)_5]^{2+}$ formed in DME, and complexes of $[Mg(THF)_6]^{2+}$, $MgCl_2(THF)_4$ and $[Mg_2(\mu\text{-}Cl_3)(THF)_6]^+$ formed within THF solvent, we calculated the length of Mg–O bond and the bond angle of ∠O–Mg–O of the complexes, as shown in Fig. 2(a), we also calculated the LUMO–HOMO value of these complexes and the energy gap value of the complexes, as shown in Fig. 2(b).

Fig. 2(a) shows the length of Mg–O bond of the complexes. $[Mg(DME)_3]^{2+}$ without chloride atoms are 2.07 Å. With the addition of Cl ions, the length of Mg–O bond first shorts to 2.06 Å, and then the length of Mg–O bond are maintained at 2.07 Å. It means that the Mg–O bond length of Mg–Cl complexes in DME solvent is relatively stable. The length of Mg–O bond of the complexes in THF solution decrease with the increase of Cl ions. We also statistic the angle between O–Mg–O in different complexes in DME and THF solutions. It can be seen that the bond angle of ∠O–Mg–O of Mg–Cl complexes in DME are maintained at about 79°, while the bond angle of THF complexes are slightly larger. In addition, we calculated the length of Mg–Cl bond in Mg–Cl complexes of DME and THF, and found that the bond lengths were concentrated between 2.4 Å and 2.6 Å, which are consistent with the data in the early literature.[33] The length of Mg–Cl bond of $MgCl_2$ salt remains at 2.26 Å, and the formation of complexes make the length of Mg–Cl bond become longer, the difference was about 0.2 Å. The bond angle between Cl–Mg–Cl of complexes in both DME and THF solvents are all about 84°. Fig. 2(b) statistics the HOMO–LUMO values of Mg–Cl complexes in DME and THF solvents. LUMO energy also represents the ability to acquire electrons. Therefore, a lower LUMO energy means a higher electron affinity, and the ability to accept electrons also enhanced. It can be seen from Fig. 2(b) that $[Mg(DME)_3]^{2+}$ has the lowest LUMO energy, indicating that $[Mg(DME)_3]^{2+}$ is the most easily oxidized compound, and it is easy to obtain electrons from the anode during discharge. A reduction in the total energy gap between HOMO and LUMO improves electrical conductivity, which speeds up electron transport.[34] The results of the energy gap are calculated with the formula (4). It can be seen from Fig. 2(b) that the energy gap of $[Mg(DME)_3]^{2+}$ (8.42 eV) and $[Mg(THF)_6]^{2+}$ (8.45 eV) complexes are the highest, and the energy gap decreases after the addition of Cl ions, which means that the addition of Cl^- improves the conductivity of each complex in the electrolyte. Finally, the energy gap value of the Mg–Cl complexes remained stable between 6.7 and 8.0 eV.

Since we still have not exactly understood whether the presence of complexes accelerate or slow down the S-reduction process, we took the S-reduction reaction process without complexes as the basic reaction formula and explored the properties of the complexes under the solvents of DME and THF

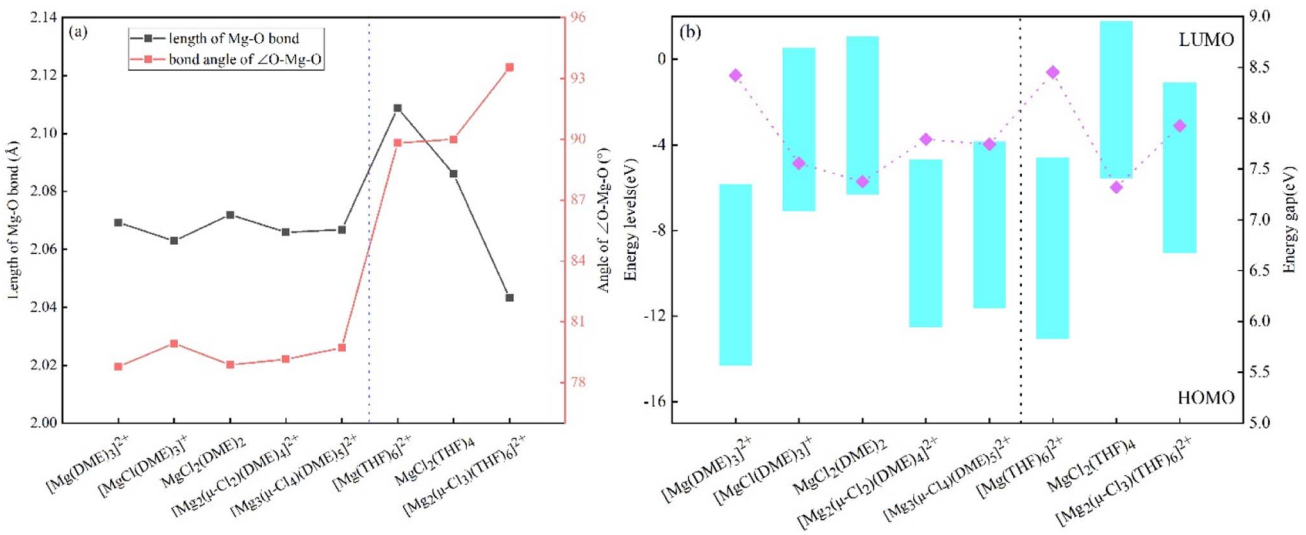

Fig. 2 (a) The length of Mg–O bond and the bond angle of ∠O–Mg–O of Mg–Cl complexes within DME and THF solvents (b) HOMO–LUMO energy-level and Energy gap of Mg–Cl complexes within DME and THF solvents.

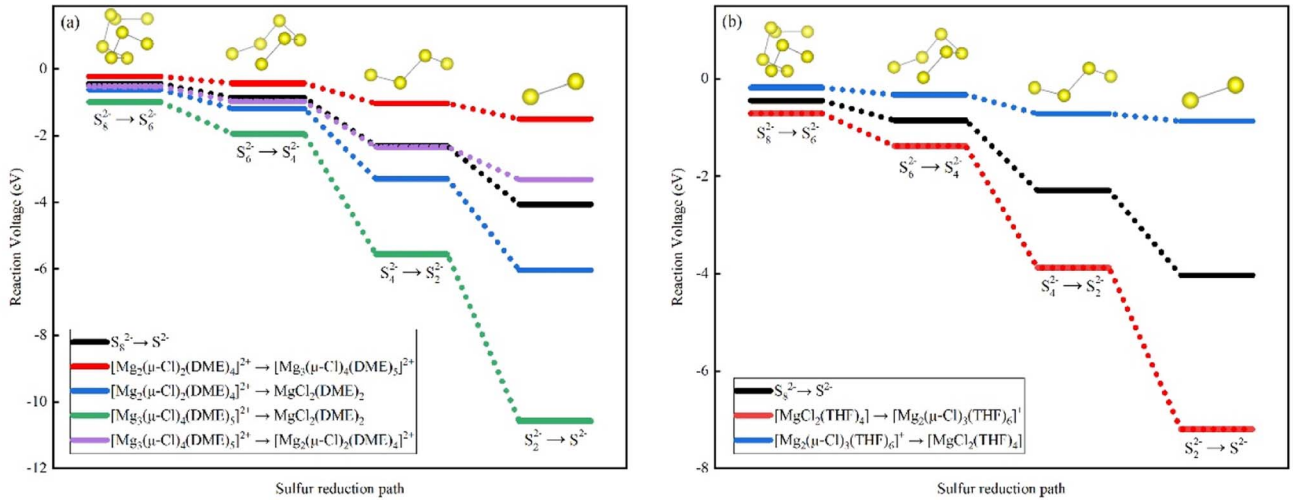

Fig. 3 Reactions of Mg–Cl complexes in (a) DME solvents and (b) THF solvents in S-reduction.

Table 12 Reaction steps of Mg–Cl complexes within DME solution during S-reduction

No.	Equation	ΔG (eV)	$\Delta G_{\text{per S}}$
R_{49}	$2[Mg_2(\mu\text{-}Cl)_2(DME)_4]^{2+} = [Mg_3(\mu\text{-}Cl)_4(DME)_5]^{2+} + 3DME + Mg^{2+}$	5.13	—
R_{50}	$[Mg_2(\mu\text{-}Cl)_2(DME)_4]^{2+} = MgCl_2(DME)_2 + 2DME + Mg^{2+}$	−3.95	—
R_{51}	$[Mg_3(\mu\text{-}Cl)_4(DME)_5]^{2+} = 2MgCl_2(DME)_2 + DME + Mg^{2+}$	−13.02	—
R_{52}	$Mg^{2+} + [Mg_3(\mu\text{-}Cl)_4(DME)_5]^{2+} + 3DME = 2[Mg_2(\mu\text{-}Cl)_2(DME)_4]^{2+}$	−5.13	—
R_{53}	$Mg^{2+} + 3S_8^{2-} + 2e^- = 3S_6^{2-} + MgS_6$	−10.69	−0.45
R_{54}	$Mg^{2+} + 2S_6^{2-} + 2e^- = 2S_4^{2-} + MgS_4$	−10.31	−0.86
R_{55}	$Mg^{2+} + S_4^{2-} + 2e^- = S_2^{2-} + MgS_2$	−9.25	−2.31
R_{56}	$Mg^{2+} + S_2^{2-} + 2e^- = S^{2-} + MgS$	−8.14	−4.07

respectively. We plotted Fig. 3 with the data from Tables 12 and 13. As shown in Fig. 3(a), sulfur spontaneously changes from S_8^{2-} to S^{2-} during the discharge process. The final product of Mg–S battery, MgS, is a solid, and accelerating the formation of the last step of the reaction product cannot extend the electrochemical performance of the battery, and improving the battery performance. In the process of charging reaction, the reaction product is transformed from solid MgS to MgS_8. According to Fig. 3(a), the bi-nuclear to tri-nuclear complex is a synthetic reaction, which is exactly the opposite of the decomposition of bi-nuclear into mono-nuclear, tri-nuclear into bi-nuclear, and tri-nuclear into mono-nuclear. According to Fig. 3(b), mono-nuclear complex to bi-nuclear complex is a synthesis reaction, and bi-nuclear to mono-nuclear complex is a decomposition reaction, and their step diagrams are just distributed on both sides of the original S-reduction reaction. We calculated with the eqn (2) and (3) in the above. From the data, it can be seen that the decomposition of Δ^2G of tri-nuclear into mono-nuclear in the DME complex is the largest, which changes from the original S-reduction of 0.41, 1.45 and 1.76 eV to 0.96, 3.62 and 5.01 eV, indicating that the driving force of the decomposition of tri-nuclear into mono-nuclear is the largest. The complexes in DME $[Mg_2(\mu\text{-}Cl)_2(DME)_4]^{2+}$ and $[Mg_3(\mu\text{-}Cl)_4(DME)_5]^{2+}$, Mg/Cl are 1 : 1 and 1 : 1.3, respectively, while the complexes in THF, $MgCl_2(THF)_4$ and $[Mg_2(\mu\text{-}Cl)_3(THF)_6]^+$, Mg/Cl are 1 : 2 and 1 : 1.5 respectively, indicating that DME solvent is suitable for low Mg/Cl ratio, and THF solvent is suitable for high Mg/Cl ratio. In contrast, the Mg/Cl ratio in DME is lower, while the Mg/Cl ratio in THF is higher. If the two solvents are mixed, then the Mg/Cl ratio of the electrolyte can be kept constant.

Table 13 Reaction steps of Mg–Cl complexes within THF solution during S-reduction

No.	Equation	ΔG (eV)	$\Delta G_{\text{per S}}$
R_{31}	$Mg^{2+} + 3[MgCl_2(THF)_4] = 2[Mg_2(\mu\text{-}Cl)_3(THF)_6]^+$	−6.32	—
R_{57}	$2[Mg_2(\mu\text{-}Cl)_3(THF)_6]^+ = 3[MgCl_2(THF)_4] + Mg^{2+}$	6.32	—
R_{58}	$Mg^{2+} + 3S_8^{2-} + 2e^- = 3S_6^{2-} + MgS_6$	−10.64	−0.44
R_{59}	$Mg^{2+} + 2S_6^{2-} + 2e^- = 2S_4^{2-} + MgS_4$	−10.21	−0.85
R_{60}	$Mg^{2+} + S_4^{2-} + 2e^- = S_2^{2-} + MgS_2$	−9.17	−2.29
R_{61}	$Mg^{2+} + S_2^{2-} + 2e^- = S^{2-} + MgS$	−8.06	−4.03

4. Conclusions

In this paper, we studied the complexes formed by ring THF and chain DME solvents in the battery and the reaction process of the complexes in the battery, and explored the role of the solute salt anion additive in the battery discharge process. It was found that $MgCl_2$, as an ideal anionic salt additive, can form mono-nuclear complex $MgCl_2(DME)_2$, bi-nuclear complex $[Mg_2(\mu\text{-}Cl)_2(DME)_4]^{2+}$ and tri-nuclear complex $[Mg_3(\mu\text{-}Cl)_4(DME)_5]^{2+}$ in DME solvent. These three kinds of complexes mono-nuclear, bi-nuclear, and tri-

nuclear are directly formed in solution in turn. The bi-nuclear complex $[Mg_2(\mu\text{-}Cl)_3(THF)_6]^+$ in THF solution is directly formed under the condition of high salt concentration, when the salt concentration is lower, the mono-nuclear complex $[MgCl_2(THF)_4]$ is formed at first, and then continues to react with $MgCl_2$ to form the bi-nuclear complex $[Mg_2(\mu\text{-}Cl)_3(THF)_6]^+$. By comparing HOMO–LUMO and energy gap values of Mg–Cl complexes in different solvents, it was found that $[Mg(DME)_3]^{2+}$ had the lowest LUMO value, so it was the most easily oxidized compound. The energy gap values of the complexes decreased after the addition of Cl^-, indicating that the addition of Cl^- increased the conductivity of each complex in the electrolyte. According the data, the synthetic reaction is exactly the opposite of the decomposition. And the decomposition of Δ^2G of tri-nuclear into mono-nuclear in the DME complex is the largest, indicating that the driving force of the decomposition of tri-nuclear into mono-nuclear is the largest. According to the different ratios of Mg/Cl in the complexes involved in S-reduction, the Mg/Cl in the complex cations $[Mg_2(\mu\text{-}Cl)_2(DME)_4]^{2+}$ and $[Mg_3(\mu\text{-}Cl)_4(DME)_5]^{2+}$ in DME are 1 : 1 and 1 : 1.3, respectively. The Mg/Cl of the complex cations $MgCl_2(THF)_4$ and $[Mg_2(\mu\text{-}Cl)_3(THF)_6]^+$ in THF are 1 : 2 and 1 : 1.5, respectively. So we speculated that DME had better performance as an electrolyte solvent in battery when the Mg/Cl ratio was low, and THF had better performance as an electrolyte solvent in battery when the Mg/Cl ratio was high. The reaction of magnesium ions in the electrolyte is very complicated, this paper mainly considers the possibility of Mg–Cl complex participating in the S-reduction reaction, which has certain limitations. In addition, although the solubility of a single $MgCl_2$ salt in DME is very small, it is difficult to be applied in practice, but relevant literature shows that the addition of $MgCl_2$ greatly improves the electrochemical performance of $Mg(TFSI)_2$/DME electrolyte solutions,[6] and $MgCl_2$ is a key component in these solutions, and the auxiliary role of TFSI anion will also be considered in future work. Overall, this study represents a significant step forward in understanding the impact of complexes on Mg–S battery performance and paves the way for further optimization.

Conflicts of interest

There are no conflicts to declare.

Acknowledgements

JBW was supported by the National Natural Science Foundation of China (No. 11047164), the National Key Laboratory of Infrared Detection Technologies (No. IRDT-23-S01), the Shanghai College Foundation for Excellent Young Teachers of China (No. gjd10023) and the Academic Program of Shanghai Municipal Education Commission (No. 11XK11 and 2011X34).

References

1 X. Zhou, *et al.*, High rate magnesium–sulfur battery with improved cyclability based on metal–organic framework derivative carbon host, *Adv. Mater.*, 2018, **30**(7), 1704166.
2 Z. Zhao-Karger, *et al.*, Performance Improvement of Magnesium Sulfur Batteries with Modified Non-Nucleophilic Electrolytes, *Adv. Energy Mater.*, 2015, **5**(3), 1401155.
3 T. Gao, *et al.*, Reversible S_0/MgS_x Redox Chemistry in a $MgTFSI_2/MgCl_2$/DME Electrolyte for Rechargeable Mg/S Batteries, *Angew. Chem., Int. Ed.*, 2017, **56**(43), 13526–13530.
4 T. Gao, *et al.*, Thermodynamics and Kinetics of Sulfur Cathode during Discharge in $MgTFSI_2$-DME Electrolyte, *Adv. Mater.*, 2018, **30**(3), 1704313.
5 H. Fan, *et al.*, Extending Cycle Life of Mg/S Battery by Activation of Mg Anode/Electrolyte Interface through an LiCl-Assisted $MgCl_2$ Solubilization Mechanism, *Adv. Funct. Mater.*, 2020, **30**(9), 1909370.
6 M. Salama, *et al.*, Structural Analysis of Magnesium Chloride Complexes in Dimethoxyethane Solutions in the Context of Mg Batteries Research, *J. Phys. Chem. C*, 2017, **121**(45), 24909–24918.
7 P. He and J. L. Schaefer, The Key Role of Magnesium Polysulfides in the Development of Mg–S Batteries, *ACS Energy Lett.*, 2022, **7**(12), 4352–4361.
8 Y. Li, *et al.*, Electrochemically-driven interphase conditioning of magnesium electrode for magnesium sulfur batteries, *J. Energy Chem.*, 2019, **37**, 215–219.
9 R. Zhang, *et al.*, An artificial interphase enables the use of Mg(TFSI)(2)-based electrolytes in magnesium metal batteries, *Chem. Eng. J.*, 2021, **426**, 130751.
10 Y. Cheng, *et al.*, Highly active electrolytes for rechargeable Mg batteries based on a Mg-2(mu-Cl)(2) (+2) cation complex in dimethoxyethane, *Phys. Chem. Chem. Phys.*, 2015, **17**(20), 13307–13314.
11 J. Yang, *et al.*, Genuine divalent magnesium-ion storage and fast diffusion kinetics in metal oxides at room temperature, *Proc. Natl. Acad. Sci. U. S. A.*, 2021, **118**(38), e2111549118.
12 A. Du, *et al.*, An efficient organic magnesium borate-based electrolyte with non-nucleophilic characteristics for magnesium–sulfur battery, *Energy Environ. Sci.*, 2017, **10**(12), 2616–2625.
13 V. O. Chaffin, M. C. Pessanha and W. A. Alves, Solvation structures formed in the $MgCl_2$:$AlCl_3$-dimethoxyethane system: A look through Raman and IR spectroscopies, *Vib. Spectrosc.*, 2019, **100**, 167–171.
14 D. Huang, *et al.*, Highly Efficient Non-Nucleophilic Mg(CF3SO3)(2)-Based Electrolyte for High-Power Mg/S Battery, *ACS Appl. Mater. Interfaces*, 2020, **12**(15), 17474–17480.
15 R. Attias, *et al.*, The Role of Surface Adsorbed Cl- Complexes in Rechargeable Magnesium Batteries, *ACS Catal.*, 2020, **10**(14), 7773–7784.
16 L. Yang, *et al.*, Hybrid $MgCl_2/AlCl_3$/Mg(TFSI)(2) Electrolytes in DME Enabling High-Rate Rechargeable Mg Batteries, *ACS Appl. Mater. Interfaces*, 2021, **13**(26), 30712–30721.
17 A. Eilmes and W. A. Alves, Theory-experiment partnership applied to the spectroscopic analysis of a promising conditioning-free electrolyte for Mg batteries, *J. Mol. Liq.*, 2022, **350**, 118528.

18 H. S. Kim, *et al.*, Structure and compatibility of a magnesium electrolyte with a sulphur cathode, *Nat. Commun.*, 2011, **2**, 427.
19 T. Liu, *et al.*, A facile approach using $MgCl_2$ to formulate high performance Mg^{2+} electrolytes for rechargeable Mg batteries, *J. Mater. Chem. A*, 2014, **2**(10), 3430–3438.
20 T. Liu, *et al.*, A fundamental study on the (mu-Cl)(3)Mg-2(THF)(6) (+) dimer electrolytes for rechargeable Mg batteries, *Chem. Commun.*, 2015, **51**(12), 2312–2315.
21 K. A. See, *et al.*, The Interplay of Al and Mg Speciation in Advanced Mg Battery Electrolyte Solutions, *J. Am. Chem. Soc.*, 2016, **138**(1), 328–337.
22 K. A. See, *et al.*, Effect of Concentration on the Electrochemistry and Speciation of the Magnesium Aluminum Chloride Complex Electrolyte Solution, *ACS Appl. Mater. Interfaces*, 2017, **9**(41), 35729–35739.
23 J. B. Moss, *et al.*, Computational Insights into Mg–Cl Complex Electrolytes for Rechargeable Magnesium Batteries, *Batteries Supercaps*, 2019, **2**(9), 792–800.
24 V. O. Chaffin and W. A. Alves, Composition dependence on the spectral behavior of magnesium aluminum chloride complex electrolytes, *J. Mol. Liq.*, 2020, **315**, 113722.
25 A. Eilmes and W. A. Alves, Combining experimental and theoretical vibrational spectroscopy to study magnesium aluminum chloride complex electrolytes, *J. Mol. Liq.*, 2021, **333**, 116053.
26 J. Xiao, *et al.*, Stable Solid Electrolyte Interphase In Situ Formed on Magnesium-Metal Anode by using a Perfluorinated Alkoxide-Based All-Magnesium Salt Electrolyte, *Adv. Mater.*, 2022, **34**(30), 2203783.
27 M. Cheng, *et al.*, Efficient single-perfluorinated borate-based electrolytes for rechargeable magnesium batteries, *Energy Storage Mater.*, 2022, **51**, 764–776.
28 J. Zhang and M. Dolg, ABCluster: the artificial bee colony algorithm for cluster global optimization, *Phys. Chem. Chem. Phys.*, 2015, **17**(37), 24173–24181.
29 J. Zhang and M. Dolg, Global optimization of clusters of rigid molecules using the artificial bee colony algorithm, *Phys. Chem. Chem. Phys.*, 2016, **18**(4), 3003–3010.
30 K. Raghavachari, Perspective on "Density functional thermochemistry. III. The role of exact exchange", *Theor. Chem. Acc.*, 2000, **103**(3–4), 361–363.
31 R. Jayan and M. M. Islam, Mechanistic Insights into Interactions of Polysulfides at VS2 Interfaces in Na–S Batteries: A DFT Study, *ACS Appl. Mater. Interfaces*, 2021, **13**(30), 35848–35855.
32 X. Jiang, *et al.*, First-principles investigation on multi-magnesium sulfide and magnesium sulfide clusters in magnesium–sulfide batteries, *RSC Adv.*, 2023, **13**(30), 20926–20933.
33 P. Wrobel, P. Kubisiak and A. Eilmes, Quantum-Chemical and Molecular Dynamics Investigations of Magnesium Chloride Complexes in Dimethoxyethane Solutions, *ACS Omega*, 2020, **5**(22), 12842–12852.
34 K. J. Shea, Applications of the intramolecular Diels-Alder reaction to the formation of strained molecules. Synthesis of bridgehead alkenes, *J. Am. Chem. Soc.*, 1982, **104**(21), 5708–5715.